Supplementary Material for

# GPS-Derived Fault Coupling of the Longmenshan Fault Associated with the 2008 Mw 7.9 Wenchuan Earthquake and its Tectonic Implications

Yanchuan Li[1], Guohong Zhang[1], Xinjian Shan[1*], Yunhua Liu[1], Yanqiang Wu[2], Hongbao Liang[2], Chunyan Qu[1], Xiaogang Song[1]

[1] State Key Laboratory of Earthquake Dynamics, Institute of Geology, China Earthquake Administration, Beijing 100029, China; yanliupcc@gmail.com (Y. L.); zhanggh@ies.ac.cn (G. Z.); liuyunhua@ies.ac.cn (Y. L.); dqyquchy@163.com (C. Q.); sxghohai@163.com (X. S.)
[2] First Crust Deformation Monitoring and Application Center, China Earthquake Administration, Tianjin 300180, China; chdqyw@126.com (Y. W.); lhb131421@126.com (H. L.)

* Correspondence: xjshan@ies.ac.cn; Tel.: +86-010-62009134

**1. Resolution Test**

We conducted a check-board test (the zebra test) to investigate the resolution of horizontal GPS velocities on $\phi$ values. Before performing the resolution test, we first estimated the average fault locking depth of the faults in the Eastern Tibetan Plateau using a grid search method (from 0.1 km to 35 km). The result shows an average fault locking depth of 22 km for major fault in Eastern Tibetan Plateau. As a result, we set the Longmenshan fault to be 30 km in depth in our model. Then we tested different models, with the distance between adjacent fault nodes varying from 20 km to 60 km (incensement was 10 km). We selected 50 km as the average distance between adjacent faults nodes, which was a trade-off between the model resolution and the minimum distance between adjacent nodes along the strike. We first designed the locking coefficient at each node to be 0.0 or 1.0 (the forward model) and calculated the GPS velocities at each station using the block's rotation parameters (Figure S3). Then, we added Gaussian noise to the calculated GPS velocities. Finally, the "noisy" GPS velocities are used to invert for the fault coupling of the LMSF (the inverted model).

The results from the resolution test indicate that our GPS data can detect the $\phi$ value variations over 50 km along the strike and 20 km at a depth of the LMSF. It is also clear from the check-board test that the $\phi$ estimates are less well resolved along the northeastern segment of the LMSF. This is expected given that few GPS sites are distributed at near field of the fault [1]. Therefore, we chose to ignore the fault coupling result along this segment.

**2. GPS Velocity Changes before and after the 2008 Mw 7.9 Wenchuan Earthquake**

The GPS velocity solutions prior to and after the 2008 Mw 7.9 Wenchuan earthquake have different sources. Discrepancies between the two solutions might arise from different processing strategies in data trade-off, frame choice, station partition and a priori constraints [2]. In order to minimize the discrepancies, we select 134 co-located GPS sites, which are at least 500 km away from the epicenter of the 2008 Mw 7.9 Wenchuan earthquake, to solve for the Euler vector between the two solutions [1]. We then rotate the velocity solution after the 2008 Mw 7.9 Wenchuan earthquake into the velocity solution prior to the 2008 Mw 7.9 Wenchuan earthquake. Thus, the two velocity solutions are within the same reference frame. The rotation of the velocity solution would not change the relative magnitude of the crustal deformation and has no effect on the calculated strain rate.

Velocity differences (the velocities after the 2008 Mw 7.9 Wenchuan earthquake minus velocities prior to the earthquake) of the co-located GPS sites, which are located within 500 km of the epicenter of the 2008 Mw 7.9 Wenchuan earthquake, contain two kinds of signals: residuals between the two velocity solutions and GPS velocity changes before and after the 2008 Mw 7.9 Wenchuan earthquake, which is related to the postseismic deformation of

the 2008 Mw 7.9 Wenchuan earthquake and the decoupling of the central northern LMSF after the 2008 Mw 7.9 Wenchuan earthquake. Compared with the velocity changes, residuals between the two velocity solutions have random features (within the error ellipses) (Figure 5a). Therefore, we ignored the effect of the residuals between the two velocity solutions and considered that the velocity differences of the co-located GPS sites were mainly contributed by the crustal deformation after the 2008 Mw 7.9 Wenchuan earthquake. The crustal deformation field (Figure 5a) after the 2008 Mw 7.9 Wenchuan earthquake has similar spatial distribution with the co-seismic deformation field of the 2008 Mw 7.9 Wenchuan earthquake [3]. The crustal deformation is obvious in near fault regions and decays rapidly toward the far field.

**3. Crustal Rotation Rate and Strain Rate**

First, we use the least-squares collocation method to interpolate the changes of velocity field by 0.5° × 0.5° to obtain a meshed velocity field (Figure 5a). Then we calculate the strain vectors at each grid points by using the spherical approximation equations. The crustal rotation rate and the principal strain rate in the Eastern Tibetan Plateau are then derived (Figure 5b). The results show that the crustal deformation after the 2008 Mw 7.9 Wenchuan earthquake mainly affects the upper crust of the eastern margin of the Tibetan Plateau, where crustal rotation occurs. Almost no deformation occurs within the Sichuan Basin.

**4. Simulation of the Postseismic Deformation Effects on Faults**

We considered two cases for the 2008 Mw 7.9 Wenchuan source faulting (Figure S4). The first case is that the hanging wall of the fault was pure thrusting component, which was driven by the postseismic deformation. The second case is that the thrusting component occurred along the southern segment and gradually transformed to the dextral strike slip component along the northern segment. Using the least-squares collocation method, as described above, to calculate the strain rate, we obtained the crustal rotation rate of the hanging wall (Figure 6). The results show that, in either case, crustal rotation of the hanging wall would lead to the fault coupling, as well as the compression and shear stress on the fault plane to be enhanced which, in turn, would result in an accumulation of elastic strain on the fault plane.

**References**


1. Li, Y.,; Shan, X.; Qu, C.; Wang, Z. Fault locking and slip rate deficit of the Haiyuan-Liupanshan fault zone in the northeastern margin of the Tibetan Plateau. Journal of Geodynamics 2016, 102, 47-57.
2. Li, Y.; Song, X.; Shan, X.; Qu, C.; Wang, Z. Locking degree and slip rate deficit distribution on MHT fault before 2015 Nepal Mw 7.9 earthquake, J. Asian Earth Sci. 2016, 119, 78-86.
3. Shen, Z.-K.; Sun, J.; Zhang, P.; Wan, Y.; Wang, M.; Bürgmann, R.; Zeng, Y.; Gan, W.; Liao, H.; Wang, Q. Slip maxima at fault junctions and rupturing of barriers during the 12 May 2008 Wenchuan earthquake, Nat. Geosci. 2009, 2, 718-724.

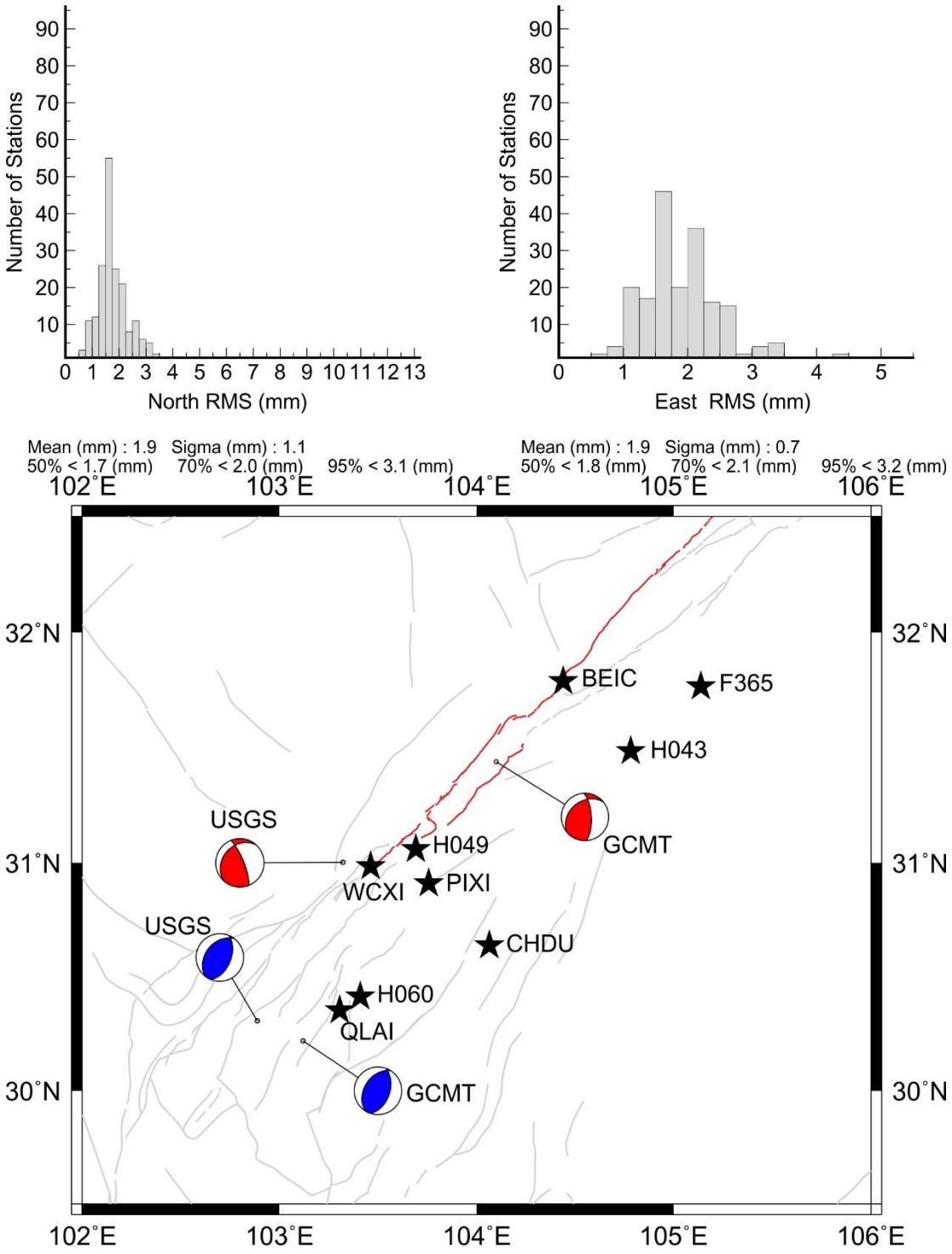
Number of Stations
North RMS (mm)
Mean (mm) : 1.9 Sigma (mm) : 1.1
50% < 1.7 (mm) 70% < 2.0 (mm) 95% < 3.1 (mm)
Number of Stations
East RMS (mm)
Mean (mm) : 1.9 Sigma (mm) : 0.7
50% < 1.8 (mm) 70% < 2.1 (mm) 95% < 3.2 (mm)
102˚E
103˚E
104˚E
105˚E
106˚E
32˚N
31˚N
30˚N
BEIC
F365
H043
USGS
GCMT
H049
WCXI
PIXI
USGS
CHDU
H060
QLAI
GCMT

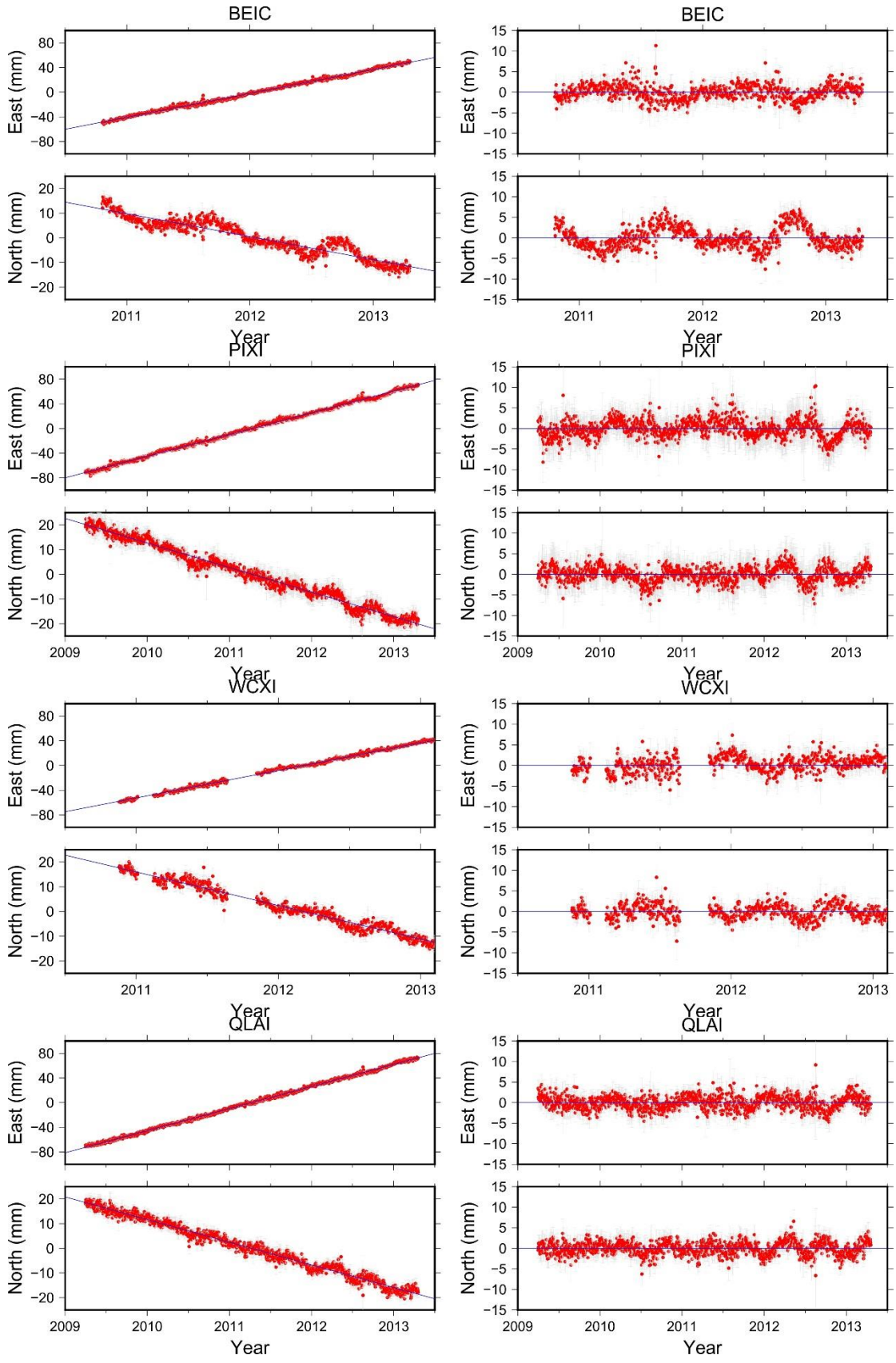
BEIC
East (mm)
North (mm)
Year
BEIC
East (mm)
North (mm)
Year
PIXI
East (mm)
North (mm)
Year
PIXI
East (mm)
North (mm)
Year
WCXI
East (mm)
North (mm)
Year
WCXI
East (mm)
North (mm)
Year
QLAI
East (mm)
North (mm)
Year
QLAI
East (mm)
North (mm)
Year

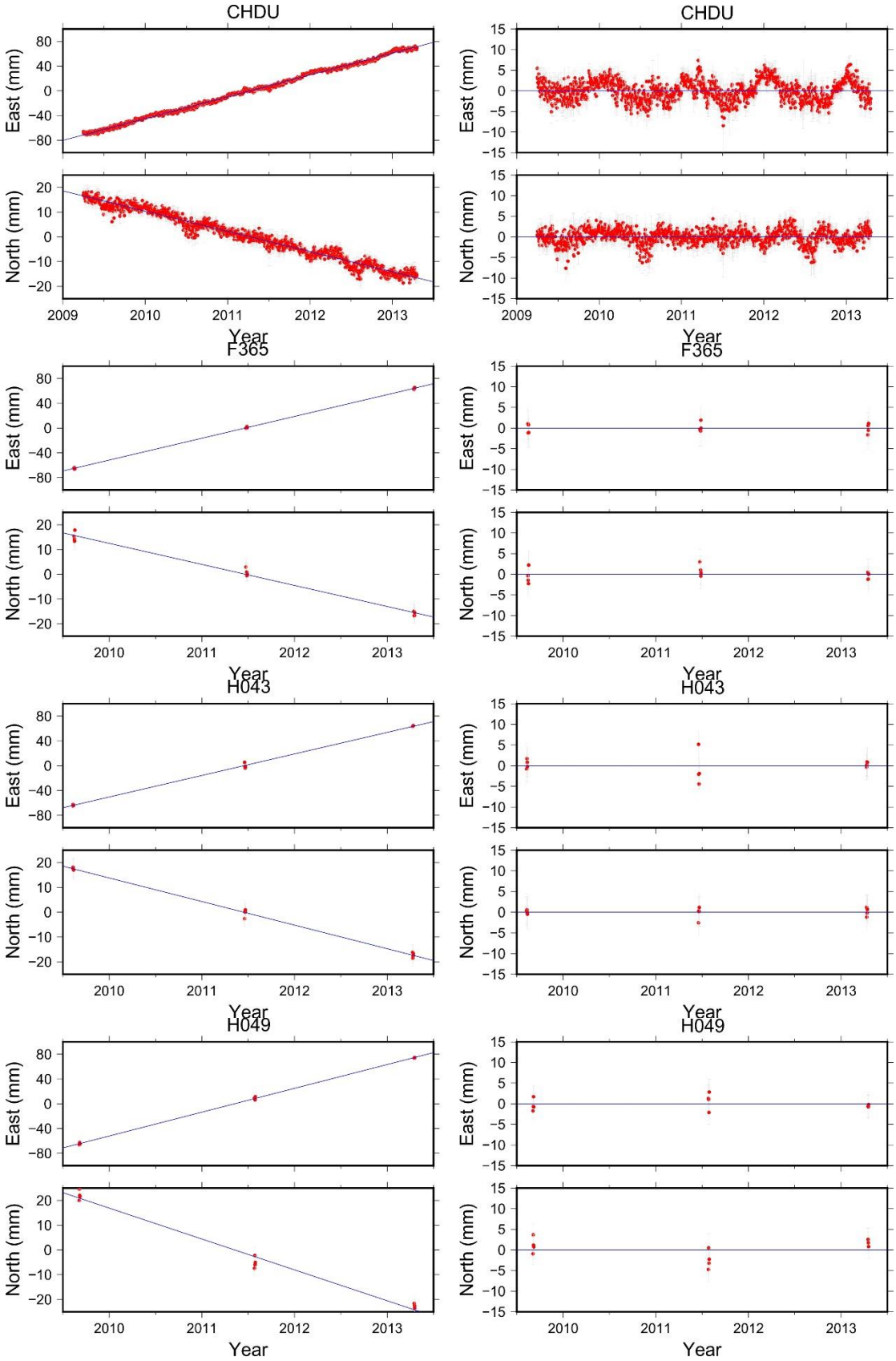


**Figure S1.** Statistic of residuals for GPS sites in the time span 2009–2013. GPS site locations (a few examples) and the corresponding time series between 2009 and 2013 are shown. The sub-figure on the left shows the original time series, and the sub-figure on the right shows the residual after removing the

linear trend. The focal mechanism shown with red and blue beach balls, which come from the USGS and Global CMT, correspond to the 2008 Mw 7.9 Wenchuan earthquake and the 2013 Mw 6.6 Lushan earthquake, respectively.

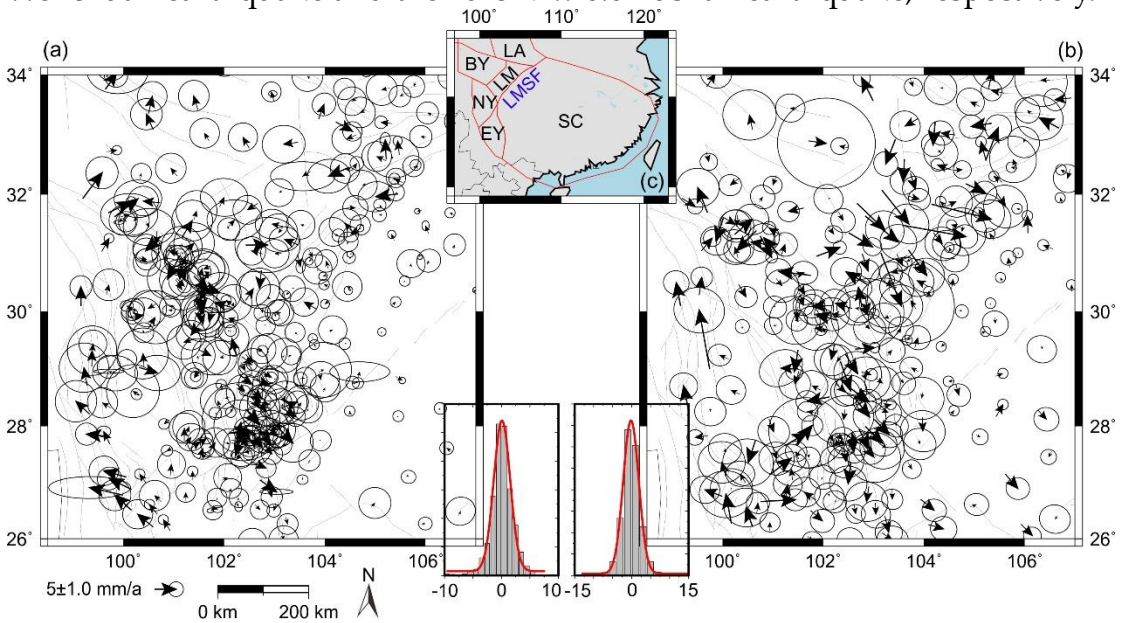


**Figure S2.** The block model and GPS velocity residuals. (**a**) Division of blocks. The red curves represent the block boundaries. (**b**) Residuals of GPS velocities (67% confidence interval) and the corresponding statistical histogram for the 1999–2007 solution. (**c**) Residuals of GPS velocities (67% confidence interval) and the corresponding statistical histogram for the 2009–2011 solution. Gray lines indicate the main active faults. Abbreviations: SC—South China block, LM—Longmen Shan block, NY—North Yunnan block, EY—East Yunnan, BY—Bayan Har block, and LZ—Lanzhou block

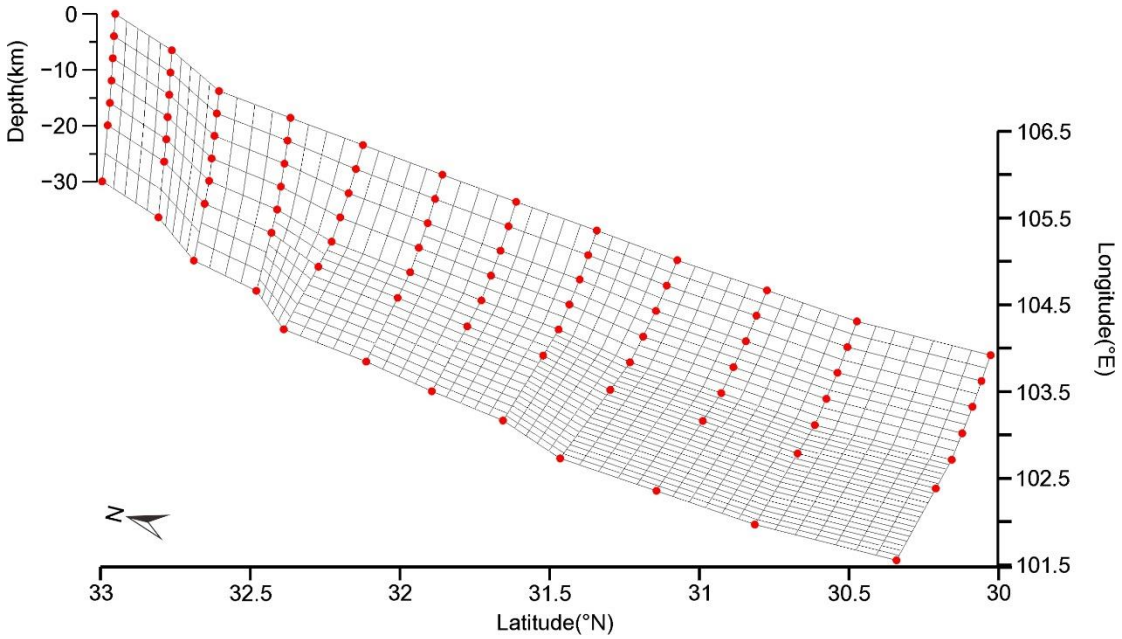


**Figure S3.** The geometry of the LMSF of our model. Red dots indicate the position of the nodes. The fault plane is further divided into 8 km × 4 km patches along the strike and dip.

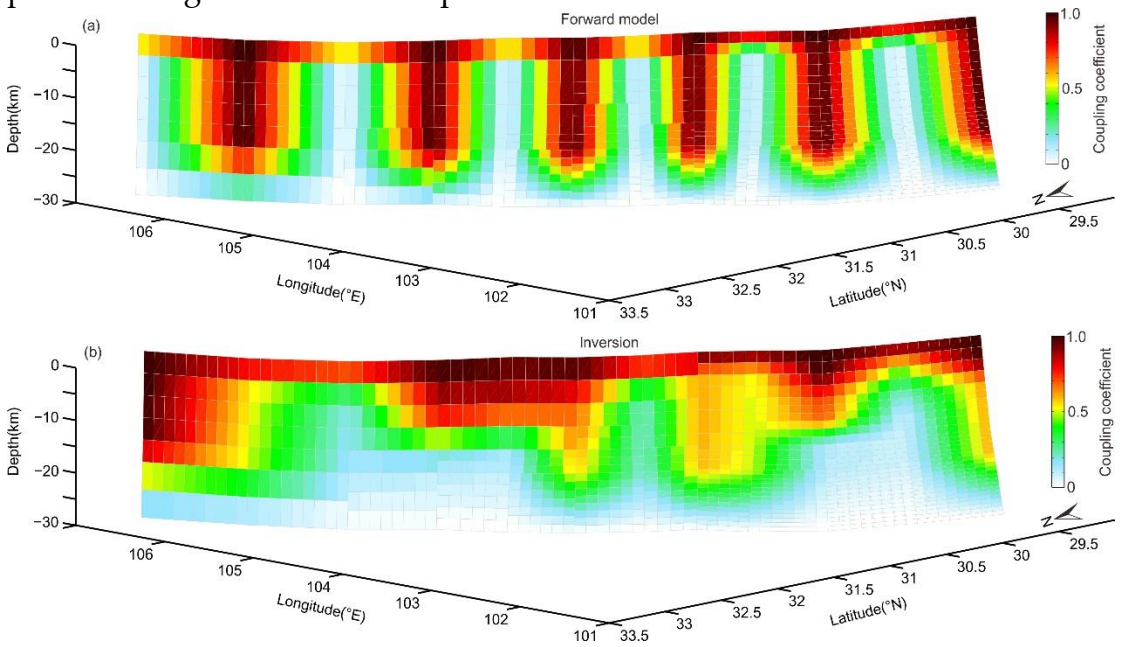


**Figure S4.** Resolution test for fault coupling modeling of the LMSF. (**a**) The input locking distribution for forward modeling. (**b**) Fault coupling recovered by inversion of the data generated by forward modeling.